

MicroRNAs accurately identify cancer tissue origin

Nitzan Rosenfeld^{1,8}, Ranit Aharonov^{1,8}, Eti Meiri^{1,8}, Shai Rosenwald^{1,8}, Yael Spector¹, Merav Zepeniuk¹, Hila Benjamin¹, Norberto Shabes¹, Sarit Tabak¹, Asaf Levy¹, Danit Lebanony¹, Yaron Goren¹, Erez Silberschein¹, Nurit Targan¹, Alex Ben-Ari¹, Shlomit Gilad¹, Netta Sion-Vardy², Ana Tobar³, Meora Feinmesser³, Oleg Kharenko⁴, Ofer Nativ⁵, Dvora Nass^{6,7}, Marina Perelman^{6,7}, Ady Yosepovich^{6,7}, Bruria Shalmon^{6,7}, Sylvie Polak-Charcon^{6,7}, Eddie Fridman^{6,7}, Amir Avniel¹, Isaac Bentwich¹, Zvi Bentwich¹, Dalia Cohen¹, Ayelet Chajut¹ & Iris Barshack^{6,7}

MicroRNAs (miRNAs) belong to a class of noncoding, regulatory RNAs that is involved in oncogenesis and shows remarkable tissue specificity. Their potential for tumor classification suggests they may be used in identifying the tissue in which cancers of unknown primary origin arose, a major clinical problem. We measured miRNA expression levels in 400 paraffin-embedded and fresh-frozen samples from 22 different tumor tissues and metastases. We used miRNA microarray data of 253 samples to construct a transparent classifier based on 48 miRNAs. Two-thirds of samples were classified with high confidence, with accuracy >90%. In an independent blinded test-set of 83 samples, overall high-confidence accuracy reached 89%. Classification accuracy reached 100% for most tissue classes, including 131 metastatic samples. We further validated the utility of the miRNA biomarkers by quantitative RT-PCR using 65 additional blinded test samples. Our findings demonstrate the effectiveness of miRNAs as biomarkers for tracing the tissue of origin of cancers of unknown primary origin.

Metastatic cancer of unknown primary origin accounts for 3–5% of all new cancer cases and is usually a very aggressive disease with poor prognosis¹. The concept of cancer of unknown primary origin comes from the limitation of present methods to identify cancer origin. Recent studies revealed a high degree of variation in clinical management in the absence of evidence-based treatment for cancers of unknown primary origin². Although many protocols have been evaluated³, they show relatively little benefit⁴. Determining the origin of tumor tissue is thus an important clinical application of molecular diagnostics⁵.

Molecular classification studies⁶ for tumor tissue origin^{6–10} have generally used classification algorithms that do not use domain-specific knowledge. All cancers were treated as equivalent, ignoring underlying similarities between tissue types with a common developmental origin. An exception of note is one study¹¹ that was based on a pathology classification tree. These studies used machine-learning methods that average effects of biological features (e.g., mRNA expression levels), an approach that is more amenable to automated processing but does not use or generate mechanistic insights.

MiRNAs have emerged as highly tissue-specific biomarkers^{12–14}, are postulated to play important roles in differentiation during development and have been tied to the development of specific malignancies¹⁵. MiRNAs appear as promising candidates for the construction of a biologically driven classification algorithm for identifying cancer

tissue of origin. Previous studies^{16–17} have paved the way for miRNA-based cancer tissue classification.

In this study, we construct an miRNA-based tissue classifier to identify the tissue origin of metastatic tumors. We developed an approach that assigns well-defined roles to individual miRNAs in classifying cancer tissue origin. We constructed the classification algorithm as a branched binary tree: in each node of the tree, classification proceeds to one of two possible branches, grouping together tissues with underlying similarities (Fig. 1). This process of coarse-to-fine specification mimics sequential processes of differentiation in embryonic development of tissues. The decision at each node is a simple binary decision that can be performed using the expression levels of a few miRNAs. This scheme is analogous to a pathologist's workup process, wherein a sample is assigned to increasingly finer subgroups through a series of differential diagnosis tests.

RESULTS

Samples and profiling

Because formalin-fixed paraffin-embedded (FFPE) archival samples are an important source for tumor material, we developed a method for extracting RNA from FFPE blocks that preserves the miRNA fraction. We compared RNA extracted from fresh-frozen, formalin-fixed or FFPE samples, and demonstrated that the RNA quantity and quality was similar for all preservation methods (Supplementary

¹Rosetta Genomics Ltd., Rehovot 76706, Israel. ²Soroka University Medical Center, Beer-Sheva 84101, Israel. ³Department of Pathology, Beilinson Hospital, Rabin Medical Center, Petah-Tikva 49100, Israel. ⁴Pathology Institute, Sourasky Medical Center, Tel Aviv 64239, Israel. ⁵Bnai-Zion Medical Center, Haifa 31048, Israel. ⁶Department of Pathology, Sheba Medical Center, Tel-Hashomer 52621, Israel. ⁷Sackler School of Medicine, Tel Aviv University, Tel Aviv 69978, Israel. ⁸These authors contributed equally to this work. Correspondence should be addressed to R.A., Rosetta Genomics Ltd., Rehovot 76706, Israel (ranit_ah@rosettagenomics.com) or I.B., Department of Pathology, Sheba Medical Center, Tel-Hashomer 52621, Israel (barshack@sheba.health.gov.il).

Received 2 January; accepted 3 March; published online 23 March 2008; doi:10.1038/nbt1392

Figure 1 Structure of the decision-tree classifier, with 24 nodes (numbered, **Table 2**) and 25 leaves. Each node is a binary decision between two sets of samples, those to the left and right of the node. A series of binary decisions, starting at node no. 1 and moving downwards, leads to one of the possible tumor types, which are the 'leaves' of the tree. A sample that is classified to the left branch at node no. 1 is assigned to the 'liver' class, otherwise it continues to node no. 2. Decisions are made at consecutive nodes using miRNA expression levels until an end-point (leaf of the tree) is reached, indicating the predicted class for this sample. For example, a sample that is classified as 'breast' must undergo the path through node nos. 1, 2, 3, 12, 16 and 17, taking the left branch at node nos. 3, 16 and 17 and the right branch at node nos. 1, 2 and 12, and no decision is needed at any of the other nodes.

In specifying the tree structure, we combined clinico-pathological considerations with properties observed in the training set data. For example, thymus samples are separated into two groups according to their histological types, differing in the expression of epithelial-related miRNAs, ostensibly due to the higher proportion of lymphocytes in B2-type tumors. The first major division (node no. 3) separates tissues of epithelial origin from tissues of other or mixed origin, a biological difference that is reflected in their miRNA expression profiles, especially in expression of the miR-141/200 family. Thymus B2 tumors are grouped here with nonepithelial or mixed tissues (on the right branch) and are separated from these later ones (**Supplementary Fig. 6**). Liver and testis were placed first in the tree because these tissues contain highly specific expression of miRNAs (hsa-miR-122a and hsa-miR-372, respectively) that can be used to easily identify them, reducing interference later. Subsequent nodes recapitulated the separation of the gastrointestinal tract from other epithelial tissues (node no. 12) using miR-194 (ref. 33) and additional miRNAs (**Fig. 2b**). Lung carcinoid tumors, as opposed to other types of lung tumors, were found to have high expression of miR-194, which may be related to their distinct biological characteristics. These tumors are therefore grouped with the gastrointestinal tissues at node no. 12 and separated from them at node no. 13 using other miRNAs (**Fig. 2a**). Cancers of the esophagus differed substantially in the expression of miRNAs used for classification according to their histological types: gastroesophageal junction adenocarcinomas were similar to samples of stomach cancer³⁴, whereas squamous samples had a strong similarity to the highly squamous head and neck cancers. Thus, the 'stomach*' class includes both stomach cancers and gastroesophageal junction adenocarcinomas; the 'head and neck*' class includes cancers of head and neck and squamous carcinoma of esophagus. GIST, gastrointestinal stromal tumors. Additional information such as patient gender or available clinical-pathological information is easy to incorporate into the tree by trimming leaves or branches (**Table 2**), without need for retraining.

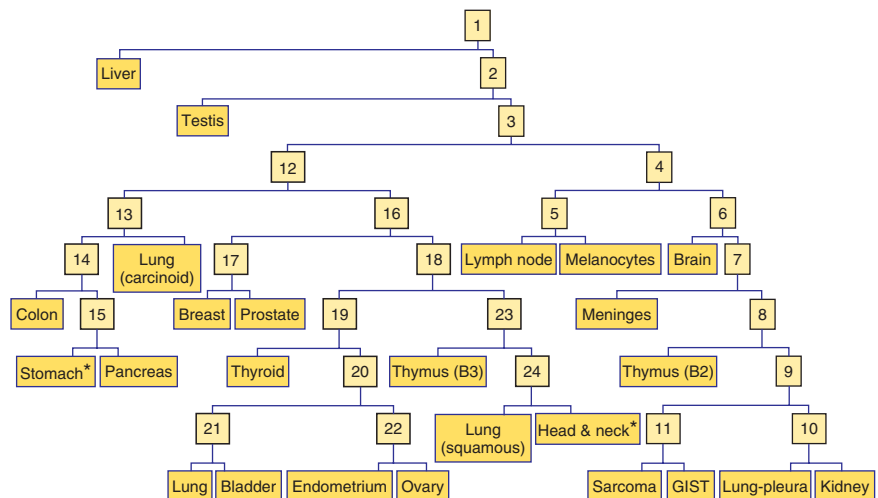


Fig. 1 online). Furthermore, the miRNA profile was stable in FFPE samples stored for as long as 11 years (**Supplementary Fig. 2** online).

MiRNA profiling was performed on miRNA microarrays¹⁸ (**Supplementary Fig. 3** online), containing probes for more than 600 miRNAs¹⁹ including all the human miRNAs in the 9th version of miRBase²⁰.

We collected and profiled 333 FFPE samples and 3 fresh-frozen samples, including 205 primary tumors and 131 metastatic tumors, representing 22 different tumor origins or 'classes' (**Table 1** and **Supplementary Table 1** online). Tumor percentage (area in section) was at least 50% for >90% of the samples. Eighty-three of the samples (~25% of each class) were randomly selected as a blinded test set. Sixty-five additional primary tumor samples (53 FFPE and 12 fresh-frozen samples, **Supplementary Table 2** online) were profiled only by qRT-PCR to validate the selected miRNAs. Overall, 401 samples are included in this study.

Comparison of primary and metastatic tumors

Owing to the difficulty of obtaining sufficient numbers of metastatic samples, this and previous studies^{7–11,16} have relied on primary tumors to augment the sample set. Differences in expression profiles between primary and metastatic samples can be expected because of underlying biological differences in the tumors, or because of contamination from neighboring tissues. These effects, which were not generally considered in previous studies, can hinder the performance of tumor classifiers on metastatic samples.

For most cancers, such as breast or colon cancer (**Supplementary Fig. 4a,b** online), we found no significant differences between primary

and metastatic tumors (**Fig. 2a,b**). In other cases, a small set of miRNAs were differentially expressed. For example, in primary tumor samples of the stomach compared to samples of stomach metastases to the lymph node, three miRNAs were significantly differentially expressed ($P < 0.001$, **Supplementary Fig. 4c,d** online). Hsa-miR-143, characteristic of epithelial layers¹², and hsa-miR-133a, which is characteristic of muscle tissue¹³, were overexpressed in the primary tumors taken from the stomach; in contrast, hsa-miR-150, which was previously identified as highly expressed in lymphocytes²¹, was present at higher levels in the metastatic samples taken from lymph nodes. In addition, samples from primary tumors such as prostate or head and neck, which often contain surrounding muscle tissue, showed high expression levels of miR-1, miR-206 and miR-133a, miRNAs that are specific to skeletal muscle¹³. We concluded that primary tumors can be used in training a classifier for metastases, but must be used with care and with attention to specific markers and to context. To reduce potential biases from these effects, we minimized the use of miRNAs in nodes where cross-contamination may have confounding effects—specifically, we avoided the use of muscle-related miRNAs (miR-1/133/206) and hsa-miR-150.

Decision-tree classification algorithm

We built a tumor classifier using the miRNA expression levels by applying a binary tree classification scheme (**Fig. 1**). This framework is set up to utilize the potential specificity of miRNAs in tissue differentiation and embryogenesis: different miRNAs may be involved in various stages of tissue specification^{22–24} and are used by the algorithm at different decision points or 'nodes'. The tree breaks up

Table 1 Cancer types, classes and histologies

Class	Cancer types and histological classifications
Bladder	Transitional cell carcinoma; mets. to brain; mets. to lung
Brain	Anaplastic astrocytoma; low grade astrocytoma; anaplastic oligodendroglioma; glioblastoma multiforme; oligodendroglioma
Breast	Infiltrating ductal carcinoma; infiltrating lobular carcinoma; mucin producing; papillary; mets. to brain; mets. to liver; mets. to lung; mets. to lymph node
Colon	Adenocarcinoma; mets. to brain; mets. to liver; mets. to lung
Endometrium	Endometrioid adenocarcinoma; serous; mets. to brain; mets. to lymph node
Head & neck*	Squamous cell carcinoma; mets. to lung-pleura; mets. to lymph node
Kidney	Clear cell carcinoma; renal cell carcinoma; mets. to brain; mets. to liver; mets. to lung; mets. to lung-pleura
Liver	Hepatocellular carcinoma
Lung	Non-small cell carcinoma; adenocarcinoma; squamous cell carcinoma; large cell; neuroendocrine; small cell; carcinoid
Lung pleura	Mesothelioma—epithelioid type; mesothelioma—sarcomatoid type
Lymph node	Hodgkin's lymphoma—classic; Hodgkin's lymphoma—nodular sclerosis; non-Hodgkin's lymphoma; diffuse large B cell
Melanocytes	Malignant melanoma; mets. to brain; mets. to lung; mets. to lymph node
Meninges	Meningioma; atypical meningioma
Ovary	Serous cystadenocarcinoma; adenocarcinoma; mets. to liver; mets. to lung-pleura; mets. to lymph node
Pancreas	Exocrine adenocarcinoma; adenocarcinoma—mucin producing; adenocarcinoma—intraductal; mets. to lung
Prostate	BPH; adenocarcinoma; mets. to lung
Sarcoma	Ewing sarcoma; fibrosarcoma; leiomyosarcoma; liposarcoma; malignant phyllodes tumor; mixed mullerian tumor; osteosarcoma; synovial sarcoma; mets. to brain; mets. to lung
Stomach*	Adenocarcinoma; mucin producing; gastroesophageal junction adenocarcinoma; mets. to liver; mets. to lymph node
GIST	Gastrointestinal stromal tumor of the small intestine
Testis	Seminoma
Thymus	Thymoma—type B2; thymoma—type B3
Thyroid	Papillary carcinoma; tall cell; mets. to lung; mets. to lymph node

The 'stomach*' class includes both stomach cancers and gastroesophageal junction adenocarcinomas; the 'head and neck*' class includes cancers of head and neck and squamous carcinoma of esophagus (see Fig. 1). 'GIST' indicates gastrointestinal stromal tumors. "mets. to s", metastases from the listed class to site s. The full list of samples with additional detail is available in **Supplementary Table 1**.

the complex multi-tissue classification problem into a set of simpler binary decisions. At each node, classes which branch out earlier in the tree are not considered, reducing interference from irrelevant samples and further simplifying the decision (Fig. 2a). The decision at each node can then be accomplished using only a small number of miRNA biomarkers, which have well-defined roles in the classification (Table 2 and Supplementary Table 3 online).

The structure of the binary tree was based on a hierarchy of tissue development and morphological similarity¹¹, which was modified by prominent features of the miRNA expression patterns (Fig. 1). For example, the expression patterns of miRNAs indicated a significant difference between lung carcinoid and other lung cancer types ($P < 10^{-10}$ for hsa-miR-194), and these are therefore separated at node no. 12 (Fig. 2a,b) into separate leaves (Fig. 1). Interestingly, an automated algorithm for dividing the data into a binary classification tree generated trees with a similar structure, yet lacked flexibility in structure and in individual node classifiers and resulted in substantially poorer performance (Supplementary Fig. 5 online).

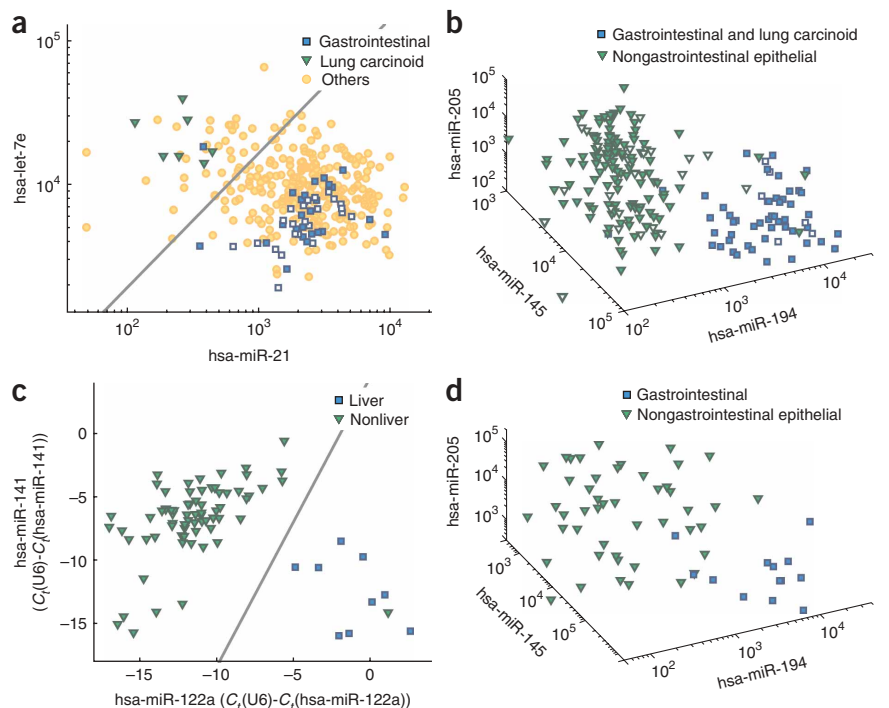
For each of the individual nodes we used logistic regression models, a robust family of classifiers that are frequently used in epidemiological and clinical studies to combine continuous data features into a binary decision (Fig. 2a and Supplementary Fig. 6 online). Because gene expression classifiers have an inherent redundancy in selecting gene features²⁵, we used bootstrapping on the training sample set as a method to select a stable miRNA set for each node. This resulted in a small number (usually 2–3) of miRNA features per node, totaling 48 miRNAs for the full classifier (Table 2 and Supplementary Table 3). Some of these miRNAs were previously identified in similar contexts (Supplementary Table 4 online).

Cross validation and high-confidence classifications

As a first step, we tested the performance of the classifier using leave-one-out cross validation (LOOCV) within the training set. LOOCV simulates the performance of a classification algorithm on unseen samples. In LOOCV the algorithm is repeatedly retrained, leaving out one sample in each round, and testing each sample on a classifier that was trained without this sample (Supplementary Table 1). The decision-tree algorithm reached an average sensitivity, or accuracy, of 78% and specificity of 99%, with notable variation between different classes (Supplementary Table 5 online). We compared the performance to that of the commonly-used K-nearest-neighbors (KNN) classification algorithm^{8,11,16}. The KNN algorithm (at the optimal $k = 3$) showed poorer performance than the tree (71% accuracy), with different classes having large differences in sensitivity between the algorithms (Supplementary Table 5, root mean square difference 25%).

In clinical practice it is often useful to assess information of different degrees of confidence^{10,11}. In the diagnosis of cancers of unknown primary origin, in particular, a short list of highly probable possibilities is a practical option when no definite diagnosis can be made. Because the decision-tree and the KNN algorithms are designed differently and trained independently, improved accuracy and greater confidence can be obtained by combining and comparing their classifications. The union of the predictions made by the two algorithms included the correct class in 85% of the cases. In 69% of the cases the two algorithms agreed, generating a single, high-confidence prediction. In 93% of these high-confidence predictions the correct class of the sample was accurately identified, with more than half of the 22 tumor classes reaching 100% sensitivity (Supplementary Table 5).

Figure 2 Binary decisions at nodes of the decision tree. (a) When training a decision algorithm for a given node, only those sample classes that are possible outcomes ('leaves') of this node are used for training. At node no. 13 (see Fig. 1), lung-carcinoid tumors (green triangles, 7 samples) are easily separated from tumors of gastrointestinal origin (blue and empty squares, 49 samples) using the expression levels of hsa-miR-21 and hsa-let-7e (with one outlier). Other samples that branch out earlier in the tree and are not well separated by these miRNAs (orange circles, 283 samples) are not considered. Notably, metastatic samples of gastrointestinal origin (empty squares, 23 samples) are distributed with the primary tumors. The solid line indicates the values of hsa-miR-21 and hsa-let-7e for which the logistic regression model of node no. 13 assigns a probability $P = 0.5$ (Supplementary Table 3). Points below the line are assigned a probability $P > 0.5$ and take the left branch (to node no. 14); points above the line take the right branch and are classified as lung-carcinoid. (b) Expression levels of hsa-miR-194, hsa-miR-145 and hsa-miR-205 at node no. 12 in the tree (Fig. 1). These miRNAs can be used to separate between the left branch of node no. 12 (blue squares, 56 samples, empty squares show metastatic samples), that is, samples from the stomach, pancreas, colon or lung-carcinoid, and other epithelial samples in the right branch of node no. 12 (green triangles, 152 samples, empty triangles show metastatic samples). (c) Validation of the miRNAs used in node no. 1 (Table 2) by qRT-PCR: liver (blue squares, 9 samples) and nonliver samples (green triangles, 71 samples) are easily separated using hsa-miR-122a and hsa-miR-141 with one outlier (Supplementary Fig. 7a,b). The signal shown for each sample is the difference in cycle threshold (C_T) between U6 and the miRNA. A larger difference means higher expression of this miRNA. Liver tumors have higher expression of hsa-miR-122a and lower expression of hsa-miR-141 (Supplementary Table 2). Line indicates the decision threshold of the logistic regression (Supplementary Fig. 7a,b). (d) Validation of the miRNAs used in node no. 12 (Table 2) by qRT-PCR: samples of gastrointestinal tumors (blue squares, 13 samples) show distinct expression levels (Supplementary Fig. 7c,d) of hsa-miR-145, hsa-miR-194 and hsa-miR-205 compared to other epithelial tumors (green triangles, 52 samples). The results obtained by qRT-PCR are very similar to those obtained by the microarray platform at this node (b and Supplementary Fig. 7d) and show similar distributions.



Classifier performance: independent blinded test-set

The most important test of a classification algorithm is on a blinded test-set. We set aside approximately one-quarter of the samples, randomly selected to represent the different classes, as an independent test set, and tested the performance of the classifiers (Table 3). The performance on the test set did not decrease compared to the performance of LOOCV in the training set (Supplementary Table 5), indicating that the classifier is robust and not over-fit. Eighty-six percent of the cases were accurately predicted by the union of the two predictors (most classes had 100% sensitivity). Among high-confidence predictions, which were two-thirds of the cases, 89% were accurately classified. Even in the blinded test-set, 16 of the 22 classes had 100% accuracy in the high-confidence predictions. Finally, we focused on the performance of the classification on the metastatic samples within the blinded test-set. Here, too, the classifier reached 85% sensitivity for high-confidence classifications. The fact that the performance on the blinded metastatic samples reached these levels of accuracy supports the approach of augmenting the training set with primary tumors when concomitantly avoiding potentially confounding markers.

Validation by quantitative RT-PCR platform

The above decision-tree algorithm, which was developed based on an array platform, assigns specific roles to miRNAs in binary decisions between groups of tissues. To rule out effects of a specific platform, we

validated the utility of a subset of these miRNAs on a high-sensitivity quantitative RT-PCR platform, using 15 of the original samples plus 65 independent samples (Supplementary Table 2). Even when using a different platform on new samples, the miRNAs maintained their expression distributions and their diagnostic roles (Fig. 2c,d) and could be used for accurate classification (Supplementary Fig. 7 online).

DISCUSSION

Gene expression profiles have recently become a basis for diagnostic, prognostic and predictive information^{26,27}, and for classification of human cancers⁶. These are particularly important for the diagnosis of cancers of unknown primary origin, which account for 3–5% of all new cancer cases in the United States⁵. Gene expression signatures of mRNA expression levels have been used for development of molecular classification algorithms to trace tumor origin^{6–11}. The 'black-box' support vector machine algorithm⁶, with >16,000 genes, reached an overall accuracy of 78% in 14 cancer classes. However, the performance of this classifier was not robust and it could not correctly identify poorly differentiated tumors. The use of the large number of data features led to some degree of over-fitting of the classifier, which did not focus on informative genes and was strongly affected by noise or irrelevant variation in gene expression. Furthermore, the design of the algorithm and the large number of genes used made it difficult to extract gene-specific biological information or to make incremental

Table 2 Nodes of the decision tree and miRNAs used in each node

Node no.	Left branch	Right branch	miRNAs used at the node
1 ^a	Liver	Node no. 2	hsa-miR-122a, hsa-miR-200c ^b
2 ^c	Testis	Node no. 3	hsa-miR-372
3	Node no. 12	Node no. 4	hsa-miR-200c, hsa-miR-181a, hsa-miR-205
4	Node no. 5	Node no. 6	hsa-miR-146a, hsa-miR-200a, hsa-miR-92a
5	Lymph node	Melanocytes	hsa-miR-142-3p, hsa-miR-509
6	Brain	Node no. 7	hsa-miR-92b, hsa-miR-9*, hsa-miR-124a
7	Meninges	Node no. 8	hsa-miR-152, hsa-miR-130a
8	Thymus (B2)	Node no. 9	hsa-miR-205
9	Node no. 11	Node no. 10	hsa-miR-192, hsa-miR-21, hsa-miR-210, hsa-miR-34b
10	Lung-pleura	Kidney	hsa-miR-194, hsa-miR-382, hsa-miR-210
11	Sarcoma	GIST	hsa-miR-187, hsa-miR-29b
12	Node no. 13	Node no. 16	hsa-miR-145, hsa-miR-194, hsa-miR-205
13	Node no. 14	Lung (carcinoid)	hsa-miR-21, hsa-let-7e
14	Colon	Node no. 15	hsa-let-7i, hsa-miR-29a
15	Stomach*	Pancreas	hsa-miR-214, hsa-miR-19b, hsa-let-7i
16	Node no. 17	Node no. 18	hsa-miR-196a, hsa-miR-363, hsa-miR-31, hsa-miR-193a, hsa-miR-210
17 ^d	Breast	Prostate	hsa-miR-27b, hsa-let-7i, hsa-miR-181b
18	Node no. 19	Node no. 23	hsa-miR-205, hsa-miR-141, hsa-miR-193b, hsa-miR-373
19	Thyroid	Node no. 20	hsa-miR-106b, hsa-let-7i, hsa-miR-138
20 ^e	Node no. 21	Node no. 22	hsa-miR-10b, hsa-miR-375, hsa-miR-99a
21	Lung	Bladder	hsa-miR-205, hsa-miR-152
22	Endometrium	Ovary	hsa-miR-345, hsa-miR-29c, hsa-miR-182
23	Thymus (B3)	Node no. 24	hsa-miR-192, hsa-miR-345
24	Lung (squamous)	Head & neck*	hsa-miR-182, hsa-miR-34a, hsa-miR-148b

^aFor samples indicated as metastasis to the liver, classification proceeds to the right branch at this node and continues to node no. 2. ^bHsa-miR-200c and hsa-miR-141 are part of one predicted polycistronic pri-miR¹⁴ and are very similarly expressed (see **Supplementary Table 4**). These two miRNAs can be used interchangeably in the tree with very slight effect on the results. Hsa-miR-200c had slightly better performance (in the training set) in node no. 1. ^cFor samples indicated as originating from a female patient, classification proceeds to the right branch at this node and continues to node no. 3. ^dFor samples indicated as originating from a female patient, classification proceeds to the left branch at this node and is classified as breast. ^eFor samples indicated as originating from a male patient, classification proceeds to the left branch at this node and continues to node no. 21. The 'stomach*' class includes both stomach cancers and gastroesophageal junction adenocarcinomas; the 'head and neck*' class includes cancers of head and neck and squamous carcinoma of esophagus (see **Fig. 1**). 'GIST' indicates gastrointestinal stromal tumors. See **Supplementary Table 3** for parameters of the logistic regression classifier at each node.

advances to this classifier. Subsequent efforts therefore aimed to use fewer features. These studies generally started with the analysis of tens of thousands of genes, followed by selection of a subset of potential biomarkers.

A pathology-motivated tree reduced the number of mRNAs analyzed, but still required 250 genes to reach accuracy of 83% when classifying up to 14 distinct cancer classes¹¹. The number of mRNAs used could be reduced below 100, but this resulted in a decrease in accuracy below 80%. One group of researchers classified 13 classes with accuracy near 90%, but required ~600 mRNAs for the task¹⁰. They were able to use <100 genes when classifying only five cancer origins. Another group classified 21 cancer classes (from 15 tissue types) with an accuracy of 85% or more using >400 genes, but the accuracy decreased sharply for fewer genes⁷. These repeated efforts suggest a trade-off between accuracy of classification, number of classes compared and the number of mRNA genes used. The limited sample-sets available for such studies make it difficult to distinguish small sets of informative genes from noise or natural variation owing to the multiple comparisons problem, especially when the initial data set contains tens of thousands of irrelevant genes. Researchers who focused intensively on the issue of feature selection, and included a large training set of nearly 500 samples, were able to substantially outperform these studies, reaching accuracy of ~90% on a broad spectrum of >30 classes (from 26 tissue origins) using a panel of 92 mRNAs⁸. This list of genes is probably strongly enriched for tissue-specific genes compared to their initial data set of 22,000 genes. However, all these classifiers used multi-feature algorithms that average effects of biomarkers and provide

little insight into the mechanistic or diagnostic role of any individual gene.

MiRNAs possess several features that make them attractive diagnostic biomarkers. MiRNAs are upstream regulators that can target large numbers of protein-coding genes. Unlike measurements of mRNA, which must be translated to protein to have a biological effect, miRNA expression levels represent more closely the functional level of the gene. An added benefit is that emerging miRNA markers can be tested for biological or therapeutic effects by generalized sequence-based methods. Notably, miRNAs show improved stability and maintain their expression profiles in archival FFPE samples²⁸ (**Supplementary Figs. 1 and 2**). One of the major characteristics of miRNAs is their marked tissue specificity and involvement in organ development^{16,22–24}. We thus postulated that a data set of miRNA expression levels would be enriched for tissue-specific markers, and would provide a fruitful starting point for the development of a tissue-of-origin classifier. Our initial data set consisted of the expression levels of several hundred miRNAs, compared to the tens of thousands of protein-coding genes used in other studies. The decision tree we described here performs a systematic search for classification decisions in which the specificity of individual miRNAs may be important. Our classifier used only 48 miRNA markers to reach an overall accuracy of ~90% among 22 tissue origins, on blinded test samples and on more than 130 metastases. This effort compares favorably with the best result so far using mRNA expression levels⁸ and will probably continue to improve as larger sample sets are collected and profiled for expression of miRNAs.

Table 3 Performance of classification on blinded test-set

	Samples		Results on blinded test-set (%)						Metastases in test set					
	N	N	Tree		KNN		Union		High conf		Union		High conf	
			Sens	Spec	Sens	Sens	Frac	Sens	N	Sens	Frac	Sens		
	Train	Test												
Bladder	4	2	0	100	0	0	100	0	1	0	100	0		
Brain	10	5	100	100	100	100	100	100	0					
Breast	19	5	60	97	60	60	80	75	4	50	75	67		
Colon	15	5	40	99	40	60	60	33	3	100	33	100		
Endometrium	7	3	0	99	67	67	0		1	100	0			
Head & neck*	23	8	100	99	88	100	88	100	0					
Kidney	15	5	100	99	80	100	80	100	2	100	50	100		
Liver	4	2	100	99	50	100	50	100	0					
Lung	44	5	80	95	100	100	80	100	1	100	100	100		
Lung-pleura	5	2	50	99	50	50	50	100	0					
Lymph-node	10	5	60	100	40	80	40	50	0					
Melanocytes	21	5	60	97	80	80	60	100	4	75	50	100		
Meninges	6	3	100	99	100	100	100	100	0					
Ovary	10	4	75	97	75	100	50	100	1	100	100	100		
Pancreas	6	2	50	100	50	100	0		0					
Prostate	6	2	100	100	100	100	100	100	0					
Sarcoma	15	5	40	99	80	80	40	100	4	75	50	100		
Stomach*	13	7	71	96	57	86	43	100	1	100	100	100		
Stromal	5	2	100	100	100	100	100	100	0					
Testis	2	1	100	100	100	100	100	100	0					
Thymus	5	2	100	98	50	100	50	100	0					
Thyroid	8	3	100	100	100	100	100	100	0					
Overall	253	83	72	99	72	86	66	89	22	77	59	85		

The number of samples in the training and test sets and the performance of classification on the blinded test-set, for each class separately and averaged over all samples. 'Sens' indicates sensitivity, 'Spec' indicates specificity. 'Tree' refers to the decision-tree algorithm, 'Union' includes the answers of both the decision-tree and KNN algorithms. 'High conf.' 'Frac' is the fraction of the samples with high confidence predictions, for which both the decision-tree and KNN algorithms agree on the classification. 'High conf. Sens' is the sensitivity among the high confidence predictions. The last columns show performance on the subset of the test set that are metastatic cancer samples. See **Supplementary Table 5** for LOOCV performance on the training set. The 'stomach*' class includes both stomach cancers and gastroesophageal junction adenocarcinomas; the 'head and neck*' class includes cancers of head and neck and squamous carcinoma of esophagus (see **Fig. 1**). GIST, gastrointestinal stromal tumors.

The decision-tree classifier follows a diagnostic workup plan for each sample that is based on biological differences. Because a large fraction of the miRNAs used in our classifier are hypothesized to be involved in tissue specification, the classification errors often point to neighboring or related tissues: colon misclassifications pointed to other digestive system organs (pancreas or stomach), whereas female reproductive-system organs (ovary, endometrium and breast) were relatively frequently intermixed, as previously observed¹¹. The tissue of origin that showed the consistently poorest performance, that is, that was most often misclassified, was bladder (**Table 3**). The most common error was misclassification as lung cancer (**Supplementary Table 1**), a misclassification that occurs in pathology practice and is further complicated by overlap in immunopositivity of lung and bladder cancer subtypes²⁹. This is likely related to the small number of samples of bladder origin in our study ($N = 6$).

The roles of specific miRNAs in our classifier are in agreement with previous findings (**Supplementary Table 4**) but also point to possible new roles and contribute to a broader picture of miRNA function. Our results also suggest that each node in the tree may be used as an independent differential diagnosis tool, for example in the identification of different types of lung cancer (**Figs. 1** and **2a,b**). The performance of the classifier with a small number of miRNAs highlights the utility of miRNAs as tissue-specific cancer biomarkers

and provides an effective means to determine the tissue origin of cancers of unknown primary origin.

METHODS

Tumor samples. Tumor samples were obtained from several sources (Sheba Medical Center, Tel-Hashomer, Israel; Soroka University Medical Center, Beer Sheva, Israel; Beilinson Hospital, Rabin Medical Center, Petah-Tikva, Israel; ABS Inc., Wilmington, Delaware, USA; Tel Aviv Sourasky Medical Center, Tel Aviv, Israel; Bnai-Zion Medical Center, Haifa, Israel; Seoul National University College of Medicine, Seoul, South Korea; Indivumed GmbH, Hamburg, Germany). Institutional review approvals were obtained for all samples in accordance with each institute's institutional review board or IRB-equivalent guidelines. For FFPE samples, initial diagnosis, histological type, grade and tumor percentages were determined by a pathologist on hematoxylin-eosin-stained slides, performed on the first and/or last sections of the sample. Samples included primary tumors, metastatic tumors and two samples of benign prostatic hyperplasia samples (BPH) that showed similar expression profile to prostate tumor samples (not shown). Nondefined samples were not included in this study. Tumor content in 90% of the FFPE samples was >50%.

RNA extraction. For frozen tissue, a sample ~0.5 cm³ in dimension was used for RNA extraction. Total RNA was extracted using the miRvana miRNA isolation kit (Ambion) according to the manufacturer's instructions. Briefly, the sample was homogenized in a denaturing lysis solution followed by an acid-phenol:chloroform extraction. Finally, the sample was purified on a glass-fiber filter.

For FFPE samples, total RNA was isolated from seven to ten 10- μ m-thick tissue sections using the miRdicatorTM extraction protocol developed at Rosetta Genomics. Briefly, the sample was incubated a few times in Xylene at 57 °C to remove paraffin excess, followed by ethanol washes. Proteins were degraded by proteinase K solution at 45 °C for a few hours. The RNA was extracted with acid phenol:chloroform followed by ethanol precipitation and DNase digestion. Total RNA quantity and quality were checked by spectrophotometer (Nanodrop ND-1000).

miRdicator array platform. Custom microarrays were produced by printing DNA oligonucleotide probes representing >600 human miRNAs. Each probe, printed in triplicate, carried up to 22-nt linker at the 3' end of the miRNA's complement sequence in addition to an amine group used to couple the probes to coated glass slides. 20 μ M of each probe were dissolved in 2 \times SSC plus 0.0035% SDS and spotted in triplicate on Schott Nexterion Slide E coated microarray slides using a Genomic Solutions BioRobotics MicroGrid II according to the MicroGrid manufacturer's directions. Fifty-four negative control probes were designed using the sense sequences of different miRNAs. Two groups of positive control probes were designed to hybridize to miRdicator array: (i) synthetic small RNA were spiked to the RNA before labeling to verify the labeling efficiency and (ii) probes for abundant small RNA (e.g., small nuclear RNAs (U43, U49, U24, Z30, U6, U48, U44), 5.8s and 5s ribosomal RNA) were spotted on the array to verify RNA quality. The slides were blocked in a solution containing 50 mM ethanolamine, 1 M Tris (pH 9.0) and 0.1% SDS for 20 min at 50 °C, then thoroughly rinsed with water and spun dry.

Cy-dye labeling of miRNA for miRdicator array. Five μ g of total RNA were labeled by ligation³⁰ of an RNA-linker, p-rCrU-Cy/dye (Dharmacon), to the 3' end with Cy3 or Cy5. The labeling reaction contained total RNA, spikes

(0.1–20 fmoles), 300 ng RNA-linker-dye, 15% DMSO, 1× ligase buffer and 20 units of T4 RNA ligase (NEB) and proceeded at 4 °C for 1 h followed by 1 h at 37 °C. The labeled RNA was mixed with 3× hybridization buffer (Ambion), heated to 95 °C for 3 min and then added on top of the miRdicator array. Slides were hybridized 12–16 h in 42 °C, followed by two washes in room temperature (25 °C) with 1× SSC and 0.2% SDS and a final wash with 0.1× SSC.

Arrays were scanned using an Agilent Microarray Scanner Bundle G2565BA (resolution of 10 μm at 100% power). Array images were analyzed using SpotReader software (Niles Scientific).

Array signal calculation and normalization. Triplicate spots were combined to produce one signal for each probe by taking the logarithmic mean of reliable spots. All data was log-transformed (natural base) and the analysis was performed in log-space. A reference data vector for normalization R was calculated by taking the median expression level for each probe across all samples. For each sample data vector S , a 2nd degree polynomial F was found so as to provide the best fit between the sample data and the reference data, such that $R \approx F(S)$. Remote data points (outliers) were not used for fitting the polynomial F . For each probe in the sample (element S_i in the vector S), the normalized value (in log-space) M_i is calculated from the initial value S_i by transforming it with the polynomial function F so that $M_i = F(S_i)$. Data in **Supplementary Table 1** and in **Figure 2a,b** was translated back to linear-space (by taking the exponent). Using only the training set samples to generate the reference data vector did not affect the results.

Logistic regression. The aim of a logistic regression model is to use several features, such as expression levels of several miRNAs, to assign a probability of belonging to one of two possible groups, such as two branches of a node in a binary decision-tree. Logistic regression models the natural log of the odds ratio, that is, the ratio of the probability of belonging to the first group (P) over the probability of belonging to the second group ($1-P$), as a linear combination of the different expression levels (in log-space). The logistic regression assumes that

$$\ln\left(\frac{P}{1-P}\right) = \beta_0 + \sum_{i=1}^N \beta_i \cdot M_i = \beta_0 + \beta_1 \cdot M_1 + \beta_2 \cdot M_2 + \dots$$

where β_0 is the bias, M_i is the expression level (normalized, in log-space) of the i th miRNA used in the decision node, and β_i is its corresponding coefficient. $\beta_i > 0$ indicates that the probability to take the left branch (P) increases when the expression level of this miRNA (M_i) increases, and the opposite for $\beta_i < 0$. If a node uses only a single miRNA (M), then solving for P results in (**Supplementary Fig. 6**):

$$P = \frac{e^{\beta_0 + \beta_1 \cdot M}}{1 + e^{\beta_0 + \beta_1 \cdot M}}$$

The regression error on each sample is the difference between the assigned probability P and the true ‘probability’ of this sample, that is, 1 if this sample is in the left branch group and 0 otherwise. The training and optimization of the logistic regression model calculates the parameters β , and the p-values (for each miRNA by the Wald statistic and for the overall model by the χ^2 difference), maximizing the likelihood of the data given the model and minimizing the total regression error

$$\sum_{\substack{\text{Samples} \\ \text{in} \\ \text{first} \\ \text{group}}} (1 - P_j) + \sum_{\substack{\text{Samples} \\ \text{in} \\ \text{second} \\ \text{group}}} P_j$$

The probability output of the logistic model is converted here to a binary decision by comparing P to a threshold, denoted by P_{TH} , that is, if $P > P_{TH}$ then the sample belongs to the left branch (‘first group’) and vice versa. Choosing at each node the branch that has a $P > 0.5$, that is, using a probability threshold of 0.5, leads to a minimization of the sum of the regression errors. However, as our goal was the minimization of the overall number of misclassifications (and not of their probability), we used a

modification that adjusts the probability threshold (P_{TH}) to minimize the overall number of mistakes at each node. For each node we optimize the threshold to a new probability threshold P_{TH} , such that the number of classification errors is minimized (**Supplementary Table 3**). Note that this change of probability threshold is equivalent (in terms of classifications) to a modification of the bias β_0 , which may reflect a change in the prior frequencies of the classes.

Stepwise logistic regression and feature selection. The original data contain the expression levels of hundreds of miRNAs for each sample, that is, hundreds of data features. In training the classifier for each node, we selected and used only a small subset of these features for optimizing a logistic regression model. In the initial training this was done using a forward stepwise scheme. The features were sorted in order of decreasing log-likelihoods, and the logistic model was started off and optimized with the first feature. The second feature was then added, and the model re-optimized. The regression error of the two models was compared: if the addition of the feature did not provide a significant advantage ($\chi^2 < 7.88$, $P = 0.005$), the new feature was discarded. Otherwise, the added feature was kept. Adding a new feature may make a previous feature redundant (e.g., if they are very highly correlated). To check for this, the process iteratively checks if the feature with the lowest likelihood can be discarded (without losing χ^2 difference as above). After ensuring that the current set of features is compact in this sense, the process continues to test the next feature in the sorted list, until features are exhausted. No limitation on the number of features was inserted into the algorithm but in most cases two to three features were selected.

The stepwise logistic regression method was used on subsets of the training set samples by resampling the training set with repetition (‘bootstrap’) so that each of the 23 runs contained about two-thirds of the samples at least once, and any one sample had >99% chance of being left out at least once. This resulted in an average of ~2–3 features per node (~4–8 in more difficult nodes). We selected a robust set of ~2–3 features per node (**Table 2**) by comparing features that were repeatedly chosen in the bootstrap sets to previous evidence (**Supplementary Table 4**) and considering their signal strengths and reliability. To further reduce possible biases from tissue contamination, miRNAs that were specifically high in one tissue (e.g., hsa-miR-145 in gastrointestinal tissues or hsa-miR-122a in liver) were balanced where possible by miRNAs that have an inverse specificity (e.g., hsa-miR-205, which is low in gastric tissues or hsa-miR-141/200c, which is weakly expressed in liver, **Fig. 2**). When using these selected features to construct the classifier, the stepwise process was not used and the training optimized the logistic regression model parameters only (**Supplementary Table 3**).

Restriction of classes by gender and liver metastases. The decision-tree framework allows easy implementation of available clinical information into the classification (**Table 2**). We used two such data: gender, and liver metastases. Samples from female patients were not allowed to be classified as originating from testis or prostate; thus, samples of female patients that reached node no. 2 were automatically classified to the right branch, and likewise the left branch (= breast) at node no. 17. Samples from male patients were not allowed to be classified as originating from endometrium or ovary and were automatically classified to the left branch at node 20. Samples that were indicated as liver metastases were not allowed to be classified as originating from liver tissue and were classified to the right branch in node no. 1. Thus, additional information is easily used without loss of generality or need to retrain the classifier.

K-nearest-neighbors (KNN) classification algorithm. The KNN algorithm calculated the distance (Pearson correlation) of any sample to all samples in the training set and classified the sample by the majority vote of the k samples that are most similar (k being a parameter of the classifier). The correlation was calculated on a predefined set of miRNAs (data features), selected by going over all pairs of tissue types (classes) and collecting miRNAs that were significantly differentially expressed between any two classes. Using only the intersection of this list with the 48 miRNAs that were used by the decision tree did not reduce the performance, highlighting the information content of these miRNAs. KNN algorithms with $k = 1, 3, 5$ were compared, and the optimal performer was selected, using $k = 3$ and the smaller set of miRNAs.

qRT-PCR. One microgram of total RNA was subjected to polyadenylation reaction as described before³¹. Briefly, RNA was incubated in the presence of poly (A) polymerase (PAP) (Takara-2180A), MnCl₂, and ATP for 1 h at 37 °C. Reverse transcription was performed on the poly-adenylated product. An oligo-dT primer harboring a consensus sequence (complementary to the reverse primer) was used for reverse transcription reaction. The primer is first annealed to the poly A-RNA and then subjected to a reverse transcription reaction of SuperScript II RT (Invitrogen). The cDNA was then amplified by real-time PCR reaction, using a miRNA-specific forward primer, TaqMan probe and universal reverse primer. The reactions were incubated for 10 min at 95 °C followed by 42 cycles of 95 °C for 15 s and 600 °C for 1 min. **Supplementary Table 2** shows raw signal threshold (C_T) values.

Figure 2c shows data normalized to U6 snRNA³². Data in **Figure 2d** were normalized by U6, transformed to linear space (by the exponent base 2), and multiplied by a constant (59,000) to shift numeric values to have the same median value as the array signals. Comparing the distributions of the three miRNAs in the two separate sample subsets (six groups in all) between the microarray and the qRT-PCR data, we obtained a mean Kolmogorov-Smirnov statistic of 0.32. Only two (of the six) groups had significantly different distributions (KS-statistic < 0.05); most groups were not significantly different by the Kolmogorov-Smirnov test.

Note: Supplementary information is available on the Nature Biotechnology website.

ACKNOWLEDGMENTS

We thank Jung-Hwan Yoon of Seoul National University College of Medicine, Seoul, South Korea. N.R. dedicates this work to the memory of Yasha (Yaakov) Rosenfeld.

AUTHOR CONTRIBUTIONS

R.A., A.A., I. Bentwich, Z.B., D.C., A.C. and I. Barshack directed research; N.R., R.A., E.M., S.R., Y.S., S.G., A.C. and I. Barshack designed experiments; N.S.-V., A.T., M.F., O.K., O.N., D.N., M.P., A.Y., B.S., S.P.-C., E.F. and I. Barshack provided samples and performed pathological analysis; E.M., M.Z., N.S., S.T., D.L. and S.G. performed experiments; N.R., R.A., S.R., Y.G. and E.S. developed algorithms; N.R., S.R., H.B. and Y.G. analyzed data; Y.S., A.L., N.T. and A.B.-A. provided bioinformatic and database support; N.R., R.A., A.C. and I. Barschack wrote the paper.

COMPETING INTERESTS STATEMENT

The authors declare competing financial interests: details accompany the full-text HTML version of the paper at <http://www.nature.com/naturebiotechnology/>.

Published online at <http://www.nature.com/naturebiotechnology/>

Reprints and permissions information is available online at <http://npg.nature.com/reprintsandpermissions>

- Pimiento, J.M., Teso, D., Malkan, A., Dudrick, S.J. & Palesty, J.A. Cancer of unknown primary origin: a decade of experience in a community-based hospital. *Am. J. Surg.* **194**, 833–7, discussion 837–8 (2007).
- Shaw, P.H., Adams, R., Jordan, C. & Crosby, T.D. A clinical review of the investigation and management of carcinoma of unknown primary in a single cancer network. *Clin. Oncol. (R. Coll. Radiol.)* **19**, 87–95 (2007).
- Hainsworth, J.D. & Greco, F.A. Treatment of patients with cancer of an unknown primary site. *N. Engl. J. Med.* **329**, 257–263 (1993).
- Blaszkyk, H., Hartmann, A. & Bjornsson, J. Cancer of unknown primary: clinicopathologic correlations. *APMIS* **111**, 1089–1094 (2003).
- Varadhachary, G.R., Abbruzzese, J.L. & Lenzi, R. Diagnostic strategies for unknown primary cancer. *Cancer* **100**, 1776–1785 (2004).
- Ramaswamy, S. *et al.* Multiclass cancer diagnosis using tumor gene expression signatures. *Proc. Natl. Acad. Sci. USA* **98**, 15149–15154 (2001).
- Bloom, G. *et al.* Multi-platform, multi-site, microarray-based human tumor classification. *Am. J. Pathol.* **164**, 9–16 (2004).
- Ma, X.J. *et al.* Molecular classification of human cancers using a 92-gene real-time quantitative polymerase chain reaction assay. *Arch. Pathol. Lab. Med.* **130**, 465–473 (2006).
- Talantov, D. *et al.* A quantitative reverse transcriptase-polymerase chain reaction assay to identify metastatic carcinoma tissue of origin. *J. Mol. Diagn.* **8**, 320–329 (2006).
- Tothill, R.W. *et al.* An expression-based site of origin diagnostic method designed for clinical application to cancer of unknown origin. *Cancer Res.* **65**, 4031–4040 (2005).
- Shedden, K.A. *et al.* Accurate molecular classification of human cancers based on gene expression using a simple classifier with a pathological tree-based framework. *Am. J. Pathol.* **163**, 1985–1995 (2003).
- Baskerville, S. & Bartel, D.P. Microarray profiling of microRNAs reveals frequent coexpression with neighboring miRNAs and host genes. *RNA* **11**, 241–247 (2005).
- Farh, K.K. *et al.* The widespread impact of mammalian microRNAs on mRNA repression and evolution. *Science* **310**, 1817–1821 (2005).
- Landgraf, P. *et al.* A Mammalian microRNA Expression Atlas Based on Small RNA Library Sequencing. *Cell* **129**, 1401–1414 (2007).
- He, L. *et al.* A microRNA polycistron as a potential human oncogene. *Nature* **435**, 828–833 (2005).
- Lu, J. *et al.* MicroRNA expression profiles classify human cancers. *Nature* **435**, 834–838 (2005).
- Volinia, S. *et al.* A microRNA expression signature of human solid tumors defines cancer gene targets. *Proc. Natl. Acad. Sci. USA* **103**, 2257–2261 (2006).
- Raver-Shapira, N. *et al.* Transcriptional activation of miR-34a contributes to p53-mediated apoptosis. *Mol. Cell* **26**, 731–743 (2007).
- Bentwich, I. *et al.* Identification of hundreds of conserved and nonconserved human microRNAs. *Nat. Genet.* **37**, 766–770 (2005).
- Griffiths-Jones, S., Grocock, R.J., van Dongen, S., Bateman, A. & Enright, A.J. miRBase: microRNA sequences, targets and gene nomenclature. *Nucleic Acids Res.* **34**, D140–D144 (2006).
- Xiao, C. *et al.* MiR-150 controls B cell differentiation by targeting the transcription factor c-Myb. *Cell* **131**, 146–159 (2007).
- Hornstein, E. *et al.* The microRNA miR-196 acts upstream of Hoxb8 and Shh in limb development. *Nature* **438**, 671–674 (2005).
- Lee, Y.S., Kim, H.K., Chung, S., Kim, K.S. & Dutta, A. Depletion of human micro-RNA miR-125b reveals that it is critical for the proliferation of differentiated cells but not for the down-regulation of putative targets during differentiation. *J. Biol. Chem.* **280**, 16635–16641 (2005).
- Sempere, L.F. *et al.* Expression profiling of mammalian microRNAs uncovers a subset of brain-expressed microRNAs with possible roles in murine and human neuronal differentiation. *Genome Biol.* **5**, R13 (2004).
- Ein-Dor, L., Kela, I., Getz, G., Givol, D. & Domany, E. Outcome signature genes in breast cancer: is there a unique set? *Bioinformatics* **21**, 171–178 (2005).
- Paik, S. *et al.* Gene expression and benefit of chemotherapy in women with node-negative, estrogen receptor-positive breast cancer. *J. Clin. Oncol.* **24**, 3726–3734 (2006).
- van de Vijver, M.J. *et al.* A gene-expression signature as a predictor of survival in breast cancer. *N. Engl. J. Med.* **347**, 1999–2009 (2002).
- Li, J. *et al.* Comparison of miRNA expression patterns using total RNA extracted from matched samples of formalin-fixed paraffin-embedded (FFPE) cells and snap frozen cells. *BMC Biotechnol.* **7**, 36 (2007).
- Parker, D.C. *et al.* Potential utility of uroplakin III, thrombomodulin, high molecular weight cytokeratin, and cytokeratin 20 in noninvasive, invasive, and metastatic urothelial (transitional cell) carcinomas. *Am. J. Surg. Pathol.* **27**, 1–10 (2003).
- Thomson, J.M., Parker, J., Perou, C.M. & Hammond, S.M. A custom microarray platform for analysis of microRNA gene expression. *Nat. Methods* **1**, 47–53 (2004).
- Shi, R. & Chiang, V.L. Facile means for quantifying microRNA expression by real-time PCR. *Biotechniques* **39**, 519–525 (2005).
- Thomson, J.M. *et al.* Extensive post-transcriptional regulation of microRNAs and its implications for cancer. *Genes Dev.* **20**, 2202–2207 (2006).
- Hino, K., Fukao, T. & Watanabe, M. Regulatory interaction of HNF1 α to microRNA194 gene during intestinal epithelial cell differentiation. *Nucleic Acids Symp. Ser. (Oxf.)*, 415–416 (2007).
- van Duijn, M. *et al.* High-resolution array comparative genomic hybridization of chromosome 8q: evaluation of putative progression markers for gastroesophageal junction adenocarcinomas. *Cytogenet. Genome Res.* **118**, 130–137 (2007).